A numerical and experimental investigation of ''inverse'' triple flames

Suresh K. Aggarwal,[a] Ishwar K. Puri, and Xiao Qin
Department of Mechanical Engineering (M/C 251), University of Illinois at Chicago, 842 West Taylor Street, Room 2039, Chicago, Illinois 60607-7022

(Received 7 June 2000; accepted 6 October 2000)

Tribrachial or triple flames represent a class of partially premixed flames that generally contain three spatially distinct but synergistically coupled reaction zones, namely a rich premixed, a lean premixed, and a nonpremixed reaction zone. The generally considered flow arrangement for burner-stabilized triple flames involves a rich mixture issuing from a central port and a lean mixture from two outer ports, which we call a reference configuration (RC). Herein, we examine an inverse configuration (IC) in which a fuel-lean stream is flanked by two fuel-rich streams. The reaction zone topology in this configuration is richer and more complex compared to that in a RC flame. A numerical-experimental investigation is conducted to characterize the fundamental differences and similitude between the RC and IC methane–air triple flames in both spatial and mixture fraction based coordinates. The detailed structure of IC triple flames and their response to variations in the rich and lean equivalence ratios are examined. Finally, the transient behavior of the flames in both configurations is described. The IC and RC flames have markedly different spatial structures. In the inverse configuration, the global flame contains five reaction zones. The predicted and measured topologies of the various reaction zones are in excellent agreement. The modified mixture fraction (ξ) is found to be effective in characterizing the structure of both RC and IC flames. The scalar profiles in terms of ξ clearly illustrate the similitude between the two flames. The three reaction zones in the RC flame have a structure that is similar to that of the corresponding five reaction zones of the IC flame. The two nonpremixed (or the two rich premixed reaction zones) in the IC flames are not differentiated in terms of ξ. Both the flames are subjected to a buoyancy-induced instability at normal gravity that generates large vortex structures, which cause the reaction zones to flicker. The flame–vortex interaction is initiated in the nonpremixed reaction zone for the IC flame and in the lean premixed reaction zone for the RC flame. Consequently, the IC flame flickers with higher amplitude but lower frequency as compared to the RC flame. There is good agreement between the measured and predicted flickering frequencies for the two flames. As ϕ_{rich} is increased, the height of the two rich premixed reaction zones in the IC flames increases, their tips open, and the chemical activity in these zones decreases. While the oscillation frequency is essentially constant, the oscillation amplitude increases as ϕ_{rich} is increased. The effect of increasing ϕ_{lean} is to enhance chemical activity in the lean premixed zone. However, the two rich premixed zones and the outer nonpremixed zone are relatively unaffected by variations in ϕ_{lean}. The oscillation amplitude and frequency also remain unaffected by variations in ϕ_{lean}. © *2001 American Institute of Physics.* [DOI: 10.1063/1.1328740]

I. INTRODUCTION

Tribrachial or triple flames represent a class of partially premixed flames that generally contain three reaction zones, namely a rich premixed, a lean premixed, and a nonpremixed reaction zone. These reaction zones are spatially distinct, but are synergistically coupled due to the thermochemical and fluid dynamic interactions between them. At a fundamental level, each reaction zone is influenced by the other two so that the global flame structure is strongly dependent upon these interactions. Therefore, the effects of heat and mass transfer, differential diffusion, and flame speed and curvature are among the essential issues of interest while investigating these flames.

In recent years triple flames have received increasing attention. Numerous experimental and computational investigations that employ both counterflow and coflow configurations have been reported.[1–11] Triple flames are likely to occur in many practical situations whenever pockets of rich and lean mixtures coexist in close proximity. For instance, during the reignition of turbulent mixtures, local quenching is thought to create favorable conditions for triple flames to be established.[2] Another important role of triple flames has been shown to be in the stabilization of nonpremixed flames.[1–3,11] Here, two (one rich and the other lean) self-propagating premixed reaction zones at an edge are believed to anchor a nonpremixed reaction zone that is established in between them.

Other practical systems also involve partial premixing and triple flames. The computational study of Domingo and

[a]Author to whom correspondence should be addressed; electronic mail: ska@uic.edu

Vervisch[12] reveals the existence of triple flamelets during the autoignition of nonpremixed laminar and turbulent mixtures. More direct evidence of partially premixed combustion in diesel engines has been reported by Flynn *et al.*[13] Chomiak *et al.*[14] have conducted a numerical investigation of flame liftoff and stabilization in *n*-heptane sprays under conditions similar to those in diesel engine, and they observe that flame stabilization occurs due to the upstream propagation of ''triple'' flames. They argue that while the stabilization mechanism is quite complex, it is determined by a balance between the local convection velocity and the triplet flame propagation speed.

Our previous investigations of triple flames have considered a planar coflow configuration[15] in which a rich mixture is introduced from the inner slot and a lean mixture from the two symmetric outer slots.[6,7] In this configuration [referred to herein as the reference configuration (RC)], the triple flame contains an inner rich premixed reaction zone, an outer lean premixed zone, and a nonpremixed reaction zone where partially oxidized fuel and oxidizer (from the rich and lean zones, respectively) mix in stoichiometric proportion and undergo combustion. An alternate scenario is related to the inverse of this flow arrangement for burner-stabilized triple flames, which involves a lean mixture issuing from the central slot and a rich mixture from the two outer slots. In this inverse configuration (IC) the reaction zone topology becomes richer and more complex, and can contain as many as five reaction zones. Experimental images based on the C_2^* chemiluminescent emission from triple flames established at normal gravity in both the reference and inverse configurations are presented in Fig. 1. Both configurations are characterized by the presence of triple points at which three (lean premixed, rich premixed, and nonpremixed) reaction zones merge. Since the flames are symmetric with respect to the central plane indicated by the broken line, only a characteristic half image of each flame is presented. As indicated in Fig. 1, the inverse flame contains a lean premixed (LP) reaction zone, a nonpremixed reaction zone (NP1), two rich premixed reaction zones (RP1 and RP2), and another nonpremixed reaction zone (NP2).

There are several potential scenarios in practical combustion systems to which the inverse triple flame configuration is relevant. Any turbulent combustion system can contain a stratified flow that consists of a pocket of lean mixture surrounded by a rich mixture that is surrounded by another lean mixture. This will lead to the formation of an inverse triple flame of the type illustrated in Fig. 1. Another example pertains to a liquid rocket combustor in which a liquid oxidizer is injected into a gaseous fuel environment. In such a system, an inverse triple flame may form around or in the wake of a group of droplets, due to the formation of fuel-rich and fuel-lean regions as a result of interactions between the droplets.

II. OBJECTIVE

Therefore, this investigation is motivated by the consideration that while IC flames can be relevant to combustors burning gaseous and liquid fuels, previous investigations of triple flames have focused only on the reference configuration. By investigating IC triple flames, we can examine the extent to which conclusions made regarding RC triple flames can be generalized to other configurations. The IC flames can also be viewed as a generic class of flames in which the supply section contains an array of alternate rich and lean mixtures.

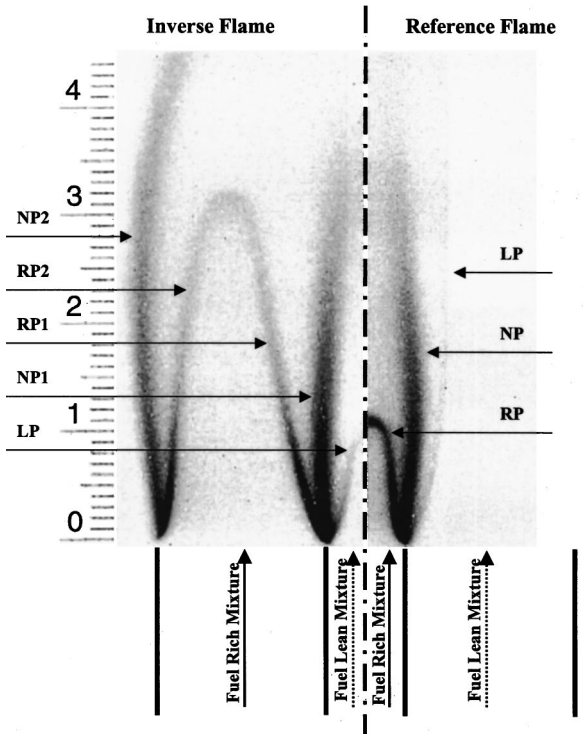

FIG. 1. Comparison of the experimental triple flame images in the reference and inverse configurations. The inverse flame (IC) is on the left-hand side and the reference flame (RC) is on the right-hand side. For both cases, the conditions are $\phi_{\text{rich}}=1.8$, $\phi_{\text{lean}}=0.38$, and $V_{\text{rich}}=V_{\text{lean}}=0.3\ \text{m s}^{-1}$. Here, ϕ_{rich} and ϕ_{lean}, respectively, denote the rich and lean equivalence ratios, and V_{rich} and V_{lean} the rich and lean stream reactant velocities through the burner. The reaction zone heights are in units of cm.

In this context, the transient behavior of IC and RC flames under 1 g conditions is also of interest. In a previous investigation,[7] we have shown that under certain conditions RC triple flames exhibit flickering whereby the outer lean premixed and the nonpremixed reaction zones are subjected to large-amplitude periodic oscillations, but the inner rich premixed reaction zone is relatively shielded from these instabilities. In the corresponding IC flames the outer rich premixed reaction zone should flicker strongly, since it interacts more closely with the ambient, while the inner lean premixed flame should be shielded from the flame flicker.

Our objective, therefore, is to characterize the structure and dynamics of normal-gravity triple flames in the inverse configuration. We first compare the RC and IC methane–air triple flame structures, and characterize interactions between the various reaction zones in each case. The results then focus on the detailed structure of IC triple flames, and the effects of rich and lean equivalence ratios on the flame structure. Thereupon, we examine the similitude and differences between the RC and IC triple flames in both spatial and

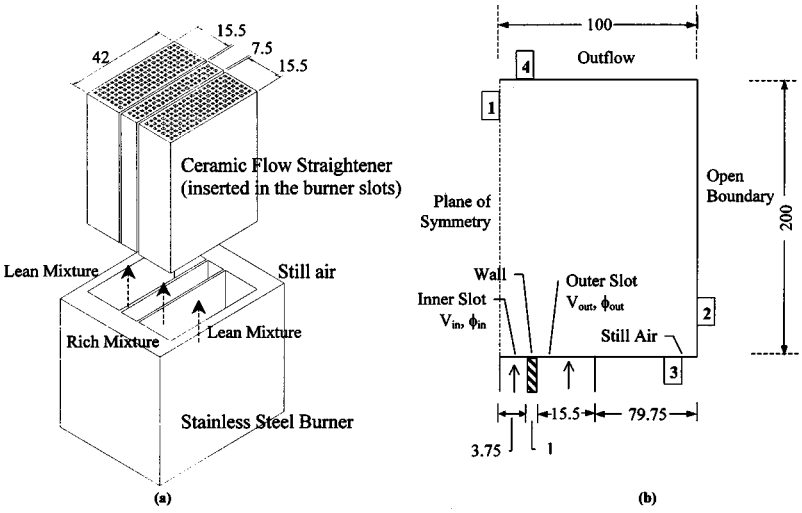

FIG. 2. Schematic diagram of (a) the slot burner, and (b) the computational domain. Dimensions are in units of mm.

mixture fraction based coordinates. Finally, the transient behavior of the flames in both configurations is characterized.

III. NUMERICAL MODEL

The numerical model simulates a triple flame established on a Wolfhard–Parker slot burner shown schematically in Fig. 2. For the reference flame, a rich mixture is introduced from the inner slot and a lean mixture from the two symmetric outer slots [cf. Fig. 2(a)], while for the inverse flame, a lean mixture is issued from the inner slot and a rich mixture from the outer slots.

A time-dependent two-dimensional model based on a direct numerical simulation methodology is employed. The CH_4–air chemistry is represented by a detailed 24-species, 81-step reaction mechanism.[16] Using Cartesian coordinates (x,y), the conservation equations can be written in the form

$$\frac{\partial(\rho\psi)}{\partial t}+\frac{\partial(\rho u\psi)}{\partial x}+\frac{\partial(\rho v\psi)}{\partial y}=\frac{\partial}{\partial x}\left(\Gamma^{\phi}\frac{\partial\psi}{\partial x}\right)+\frac{\partial}{\partial y}\left(\Gamma^{\phi}\frac{\partial\psi}{\partial y}\right)+S^{\phi}.$$

Here ρ represents the density and u and v the transverse (x) and axial (y) velocity components, respectively. The general form of this equation represents either of the mass, momentum, species, or energy conservation equations, depending upon the variable used in place of ψ. The gravitational acceleration term is included in the axial momentum equation. The transport coefficient Γ^{ϕ} and the source terms S^{ϕ} appearing in the governing equations are provided in Ref. 4. The set of governing equations is completed by introducing the global species conservation equation and the state equation. The thermodynamic and transport properties appearing in the above-mentioned equations are considered to be temperature and species dependent. A detailed algorithm, similar to that in CHEMKIN,[17] is employed to calculate these properties.

The computational model is based on an algorithm developed by Katta *et al.*[18] The algorithm employs an implicit formulation to solve the unsteady gas-phase equations. The governing equations are integrated by using a ''finite control volume'' approach with a staggered, nonuniform grid system (131×88). The computational domain is shown in Fig. 2(b). In order to minimize the effects of any outside disturbances, the computational boundaries in both the axial and transverse directions are located sufficiently far from the physical domain. Grid lines are clustered near the flame surfaces to resolve the steep gradients of the dependent variables. An iterative alternating direction implicit technique is used for solving the resulting (N_s+3) sets of algebraic equations. A stable numerical-integration procedure is achieved by coupling the species and energy equations through the chemical-reaction source terms. Further details about the numerical procedure, validation, and the treatment of boundary conditions are provided elsewhere.[18,19]

Measurements. Atmospheric methane–air triple flames are established using a Wolfhard–Parker slot burner that contains a central slot and two symmetric outer slots. The burner has been described in detail elsewhere.[7] Ceramic inserts are used to straighten and laminarize the flow in the slots. The rectangular burner geometry provides symmetrical two-dimensional flames. The velocities and equivalence ratios in the inner and outer slots can be controlled independently.

Images of the flame chemiluminescence from unsteady inverse triple flames were recorded using a high-speed video (Kodak EktaPro) system with a 4 ms exposure time at 250 Hz. In the case of unsteady flames, roughly 30 high-quality images could be recorded during one flickering cycle at this rate. The flickering frequency was measured from the recorded images obtained using the high-speed video camera.

IV. RESULTS AND DISCUSSION

A. Validation

We have previously reported measurements of RC triple[6,7,20] and double flames.[15] The measurements included those of chemiluminescent emission, temperature using holographic interferometry, and velocity based on particle image velocimetry and laser Doppler velocimetry. This allowed for a detailed validation of our numerical model, which compared the measured and predicted velocity and temperature

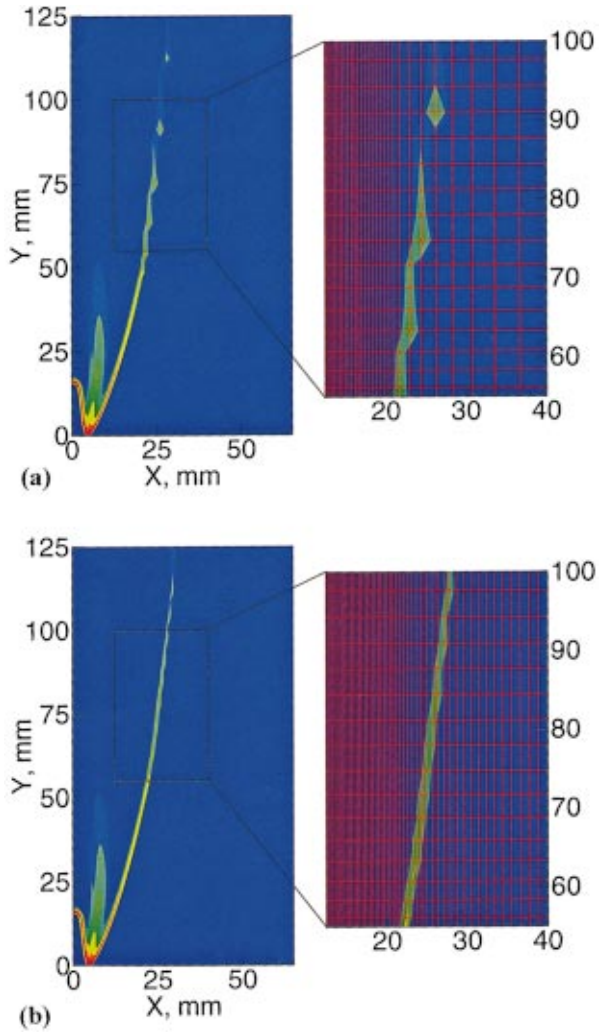

FIG. 3. (Color) Comparison of the heat release rate contours for a RC triple flame computed using two different grids: (a) 131×88 and (b) 131×108. The conditions are $\phi_{\text{rich}}=1.8$, $\phi_{\text{lean}}=0.38$, and $V_{\text{rich}}=0.3\ \text{m s}^{-1}$ and $V_{\text{lean}}=0.7\ \text{m s}^{-1}$ and zero gravity.

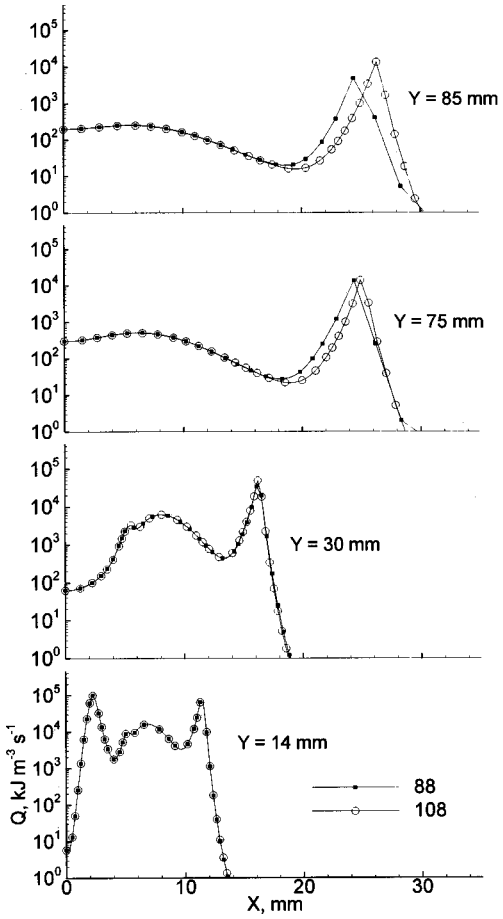

FIG. 4. Comparison of the heat release rate profiles at four transverse locations; i.e., $Y=14$, 30, 75, 85 mm, for two different grids: (a) 131×88 and (b) 131×108.

fields,[6] the experimentally obtained C_2^* chemiluminescent emission with the spatial distribution of predicted heat release rates,[6,7,15] and the measured and predicted flickering frequencies and unsteady reaction zone topologies for a 1 g triple flame.[7]

B. Grid independence

Detailed discussion of the grid dependence of the numerical results for both steady and unsteady triple flames has been provided in Ref. 19. A representative result showing the effect of local grid refinement on the computed flame structure is presented in Fig. 3. The heat release rate contours for two different grids indicate that there is essentially no difference in the triple flame structure predicted by the two grids; the global locations of the three reaction zones are nearly identical. However, the structure of the outer lean premixed zone can be made smoother by using local grid refinement, which is implemented herein.

More quantitative results on the effect of grid refinement on the computed flame structure are presented in Fig. 4,

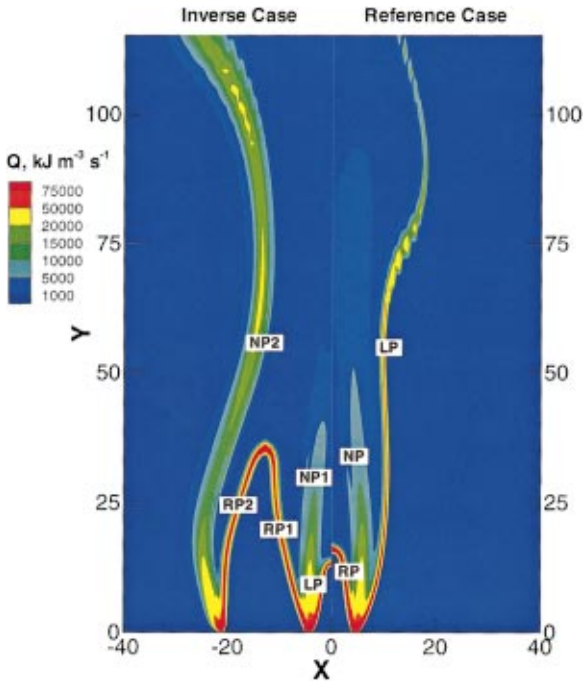

FIG. 5. (Color) Comparison of the simulated IC and RC triple flames in terms of the volumetric heat release rate contours. The conditions correspond to those for the flames discussed in the context of Fig. 1.

TABLE I. Values of three dependent variables in the lean premixed zone ($X=26.13$ mm and $Y=91.03$ mm) for two different grids.

	131×108	131×88	% change
Temperature (K)	1335	1297	2.8
Vertical velocity (m/s)	0.368	0.372	1.0
O_2 mass fraction (%)	11.59	11.96	3.2

which compares the heat release rate profiles in the transverse direction for the two grids. At lower axial locations ($Y=14$ and 30 mm), where the triple flame is characterized by the presence of three reaction zones and interactions between them, the two grids yield identical results. However, at higher axial locations, where the outer lean premixed zone is present, the predictions exhibit some grid dependency. With local grid refinement, the spatial resolution of the lean premixed reaction zone is enhanced, and this zone is shifted slightly away from the centerline. This shift, however, has no effect on the rich premixed and the nonpremixed reaction zones. The quantitative effect of grid refinement on the local values of the three dependent variables in the lean premixed zone is presented in Table I. As the grid is refined from 131×88 to 131×108, the temperature and oxygen mass fraction change by about 3% while the axial velocity changes by 1%. Note that for the finer grid, the grid size in the outer lean premixed zone is reduced by a factor of 3.

The effect of grid refinement on unsteady flame simulations was also quantified. Both the global and detailed temporal characteristics of the computed triple flame were found to be essentially grid independent. For example, the amplitude of oscillation was found to be nearly identical for the two grids, while the computed frequencies for the coarse and fine grids were 9.04 and 9.17 Hz, respectively. The measured frequency for the same case was 8.9 Hz. The effect of temporal step size on the computed flame has been reported in our previous investigation.[7]

C. Global flame structure

Figure 1 presents the global structure of RC (right) and IC (left) triple flames in terms of the C_2^* chemiluminescent emission. The flow conditions are described in the caption for Fig. 1. Since the flow is symmetric with respect to the centerline at $X=0$ (indicated by the broken line), only half of the domain is presented. The C_2^* emission signal is confined to relatively thin sheet-like reaction zones. Images of the corresponding flames obtained from numerical simulations conducted under identical conditions are presented in terms of heat release rate contours in Fig. 5.

Since the dimensions of the inner and outer slots are different, the overall equivalence ratio is different for the two cases; $\phi_{\text{overall}}=0.64$ for the RC flame and it is 1.51 for the IC flame. Moreover, the Froude numbers ($\text{Fr}=v_{\text{in}}/(\text{gL})^{1/2}$) for the two cases are different, since the relevant length scales are different. For the reference flame, the Froude number based on the inner slot width is 1.11, whereas for the inverse flame its value based on the outer slot width equals 0.68. Consequently, the inverse flame is expected to have higher propensity for flickering as compared to the reference flame. This was confirmed by both measurements and simulations, which indicated that the oscillation amplitude for the inverse flame is significantly higher than that for the reference flame.

The IC and RC flames (depicted in Figs. 1 and 5) have markedly different spatial structures. The RC flame exhibits a typical triple flame structure with a nonpremixed reaction zone (NP) located in between the rich premixed (RP) and lean premixed reaction zones (LP). As previously reported,[7] the inner rich premixed flame is relatively stable for this flame, while the outer lean premixed flame tends to flicker.

In the inverse configuration, the global flame contains five reaction zones. (Since the flame contains five reaction zones, it is perhaps more appropriate to call it a quintuple flame, rather than a triple flame. However, this may be confusing in the context of comparing the flames in two different configurations.) The first three, namely a lean premixed zone (LP), a nonpremixed zone (NP1), and a rich premixed zone (RP1), are stabilized at the thin wall separating the inner and outer slots. These three zones constitute a triple flame that is analogous to the RC triple flame. The nonpremixed reaction zone (NP1) is established where excess air and partially oxidized fuel, respectively, from the lean (LP) and rich (RP1) premixed zones meet in stoichiometric proportion. The outer two reaction zones, i.e., the rich premixed zone (RP2) and the nonpremixed zone (NP2), form a double flame, stabilized at the edge of the outer slot. As reported by Shu *et al.*,[5,15] the nonpremixed zone (NP2) is established due to the burning of partially oxidized fuel in ambient air. The partial oxidation of fuel occurs in the rich premixed zone RP2.

It is important to note that the flame structure in both the RC and IC configurations is strongly influenced by the ambient, which is considered to be quiescent and containing air. The presence of ambient air has a much stronger influence on the IC flame compared to that on the RC flame. For example, if the ambient were assumed to consist of only nitrogen, the IC flame would contain only three reaction zones, namely LP, NP1, and RP1. Consequently, it would be important to characterize the effect of replacing ambient air by ambient nitrogen on the structure of RC and IC flames.[21] We intend to examine this issue in a future investigation.

Figure 6 contains a comparison of the phase-matched experimental and simulated images for an IC flame established at conditions corresponding to Figs. 1 and 5. The simulated image is based on the CHO mass fraction contour (since CHO has been reported to be an excellent marker of flame heat release[22]), while the experimental image presents the C_2^* chemiluminescent emission signal (which we have previously found to correlate with the reactant flow rates and, thereby, the overall heat release[15]). The predicted and measured topologies of the various reaction zones are in excellent agreement, although there is a slight difference with respect to the heights of the inner lean premixed reaction zone.

A comparison of the IC and RC flames in terms of temperature and velocity fields is presented in Fig. 7. The veloc-

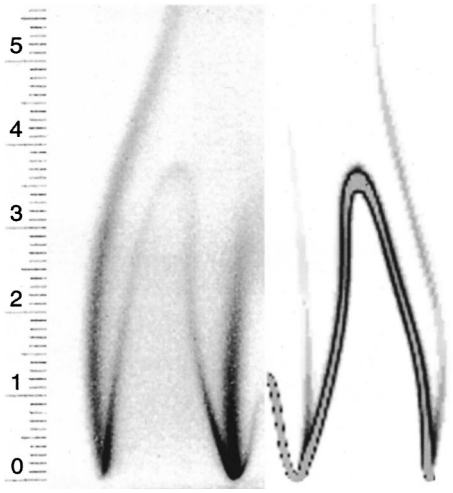

FIG. 6. Comparison of the experimental (left-hand side) and simulated (right-hand side) flame images for the IC triple flame considered in the context of Figs. 1 and 4.

ity profiles clearly exhibit the effect of buoyancy, since the flow is accelerated in the high temperature regions as a result of the density gradients. Entrainment from the surroundings in the RC flame occurs into the LP and the NP reaction zones. Consequently, the velocity vectors in the lean premixed and nonpremixed regions are directed toward the centerline, and the flame becomes globally more compact. The RC flame exhibits a single high temperature region that occurs between the nonpremixed and rich premixed reaction zones. In the inverse configuration, there are two high temperature regions surrounded by cooler gas, one between the lean premixed (LP) and the central nonpremixed (NP1) reaction zones, and the other between the outer rich premixed (RP2) and the outermost nonpremixed (NP2) reaction zones.

Buoyant transport is unaffected by the configuration. In the IC flame the buoyant convection induced by the high temperature region closest to the centerline is similar in nature to that in the RC flame. Here, velocity vectors are directed toward the centerline, causing the central nonpremixed (NP1) and the innermost rich premixed (RP1) reaction zones to assume a convex curvature, as shown in Fig. 5. The asymmetry of the entire rich premixed reaction zone (encompassing RP1 and RP2) is partly attributable to this effect, and partly to the differences in interactions between the various reaction zones. The outer high temperature region influences the shape of the outer nonpremixed (NP2) reaction zone and the air entrainment from the otherwise quiescent ambient into the flame. Gravity has a relatively stronger influence on the IC flame due to its lower Froude number than on the RC flame. This is confirmed by examining the velocity field in Fig. 7, which indicates that the maximum velocity in the IC flame is noticeably larger (4.27 compared to 3.45 $m\,s^{-1}$) than that in the RC flame. Another important effect of buoyant acceleration is the presence of an absolute instability, which induces well-organized flame oscillations. This aspect will be discussed later.

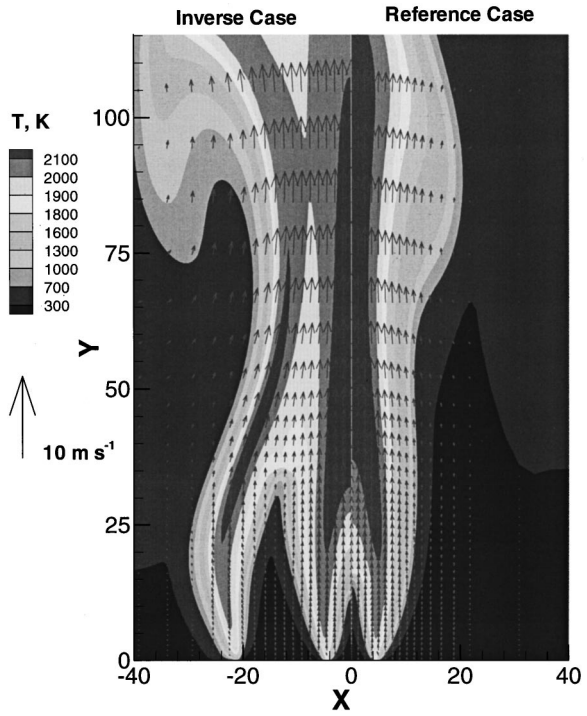

FIG. 7. Comparison of the RC and IC triple flames in terms of the temperature and velocity fields. The conditions correspond to those for the flames discussed in the context of Fig. 1.

D. Combustion efficiency

The two flames differ significantly with respect to the total fuel consumption and combustion efficiency. Figure 8 presents the axial profiles of major species' mass fractions averaged along the transverse direction. In accord with the results presented previously, the profiles exhibit significant differences regarding the spatial structures of the two flames. The methane mass fraction profiles indicate that while the methane is completely consumed in the IC flame, some methane remains unburnt at the burner exit for the RC flame. This can be attributed to the fact that the outer lean premixed reaction zone has an open tip for the RC flame, while the corresponding rich premixed reaction zone for the IC case has a closed tip. It is important to note that the total amount of fuel injected is significantly higher for the IC case compared to that for the RC case. As a consequence, the mass fractions of CO_2 and H_2O at the burner exit are much higher for the IC flame. However, the ''intermediate fuel'' species' (CO and H_2) profiles indicate the averaged mass fractions of these species at the burner exit are significantly higher for the IC flame compared to those for the RC flame. This implies that a relatively large amount of CO and H_2 leak through the outer nonpremixed reaction zone (NP2) and remain unburnt at the burner exit for the IC flame.

In summary, the consumption of methane is more efficient for the RC flame than for the IC flame, but relatively significant amounts of unburnt CO and H_2 (intermediate fuel species) leak through the IC flame. This implies a lower combustion efficiency for the IC flame. To examine this aspect, the actual and theoretical volumetric heat release rates were computed for the two flames. Based on the total fuel flow rates, the theoretical heat release rates assuming that all

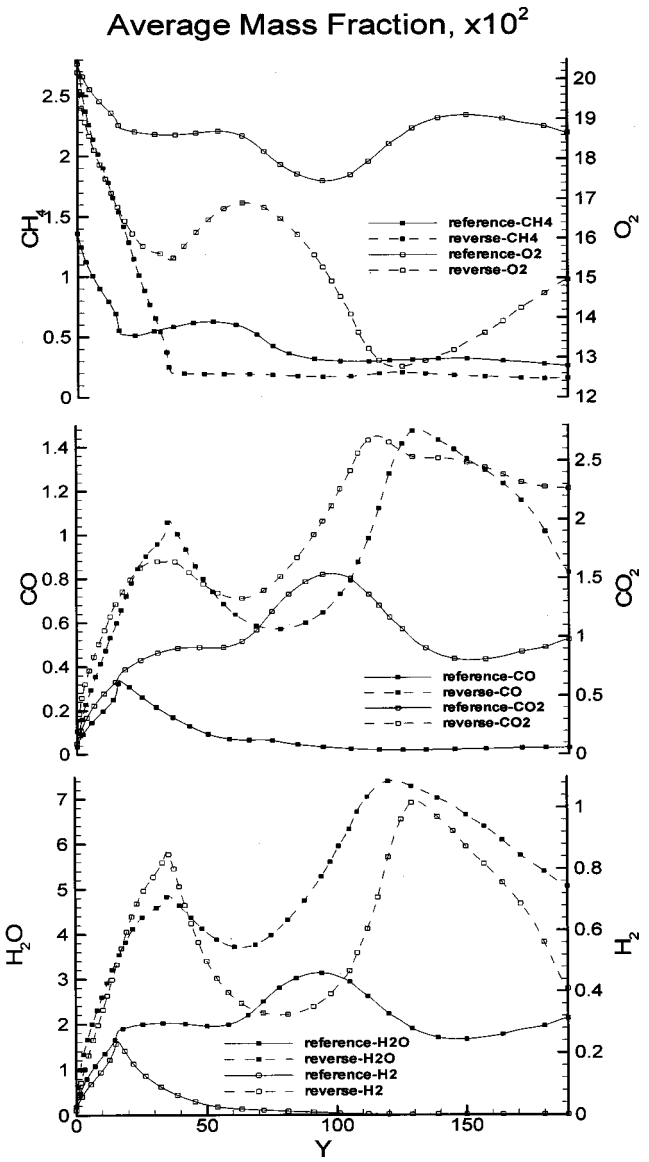

FIG. 8. Comparison of RC and IC flames in terms of the average mass fractions of major species plotted vs the axial distance. The term ''reverse'' refers to the inverse configuration (IC). Conditions correspond to those of Fig. 1.

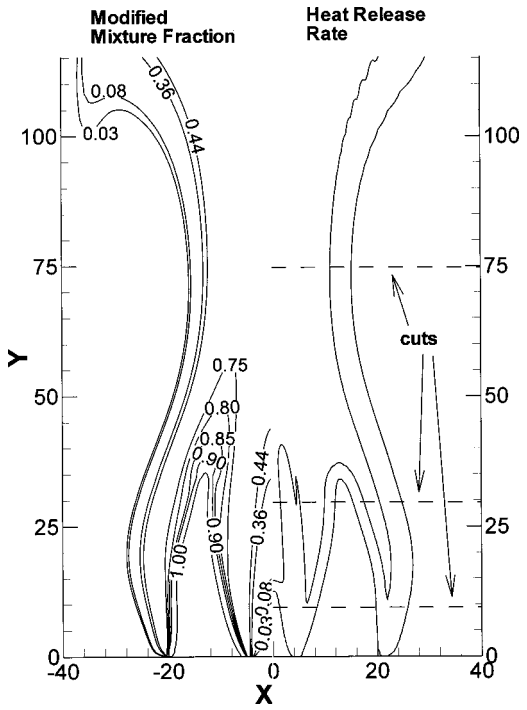

FIG. 9. Flame structure in terms of the modified mixture fraction and heat release rate contours for the IC flame corresponding to the conditions of Fig. 1.

of the methane is converted to CO_2 and H_2O are 1.01 and 2.2 kJ s^{-1} for the RC and IC cases, respectively. The actual heat release rates obtained from the predicted heat release rate profiles are, respectively, 0.93 and 1.93 kJ s^{-1}, yielding combustion efficiencies of 91.8% and 87.1% for the RC and IC flames, respectively, which is in correspondence with the leakage of CO and H_2

E. State relationships and similitude

We have found that the conserved scalar approach based on a modified mixture fraction is effective (1) in characterizing state relationships and (2) for examining the similitude between partially premixed flames in different configurations.[4–7] We follow a similar approach here to examine the similitude between the inverse and reference flames. The modified mixture fraction is defined as $\xi=(Z-Z_l)/(Z_r-Z_l)$, where Z denotes the local mass fraction of an elemental species (herein taken as the local nitrogen mass fraction) and the subscripts r and l represent conditions at the boundaries of the rich and lean regions, respectively.

Figure 9 presents the modified mixture fraction (left) and heat release rate (right) contours for the IC triple flame established at conditions corresponding to Fig. 1. Although there are differences in the contour shapes, both the modified mixture fraction and heat release rate contours are effective in identifying the five reaction zones, and suggest that the thermochemistry and state relationships are well correlated. In terms of the ξ contours, the inner lean premixed reaction zone (LP) lies in the range of $0.04<\xi<0.08$, both of the inner and outer nonpremixed zones (NP1 and NP2) between $0.36<\xi<0.44$, and both of the rich premixed zones between $0.75<\xi<0.9$. The contours also indicate that the five distinct reaction zones in the physical space are reduced to three in ξ space, since the two nonpremixed zones (NP1 and NP2) and the two rich premixed zones (RP1 and RP2) are represented by the same ξ contours, respectively. This again underscores the effectiveness of the modified mixture fraction in characterizing triple flames in different configurations.

Figure 10 presents state relationships for the temperature, OH (a radical species), and CO (an intermediate partially oxidized species) mass fractions with respect to ξ along three transverse locations for the RC and IC triple flames. In order to identify the location of the various reaction zones, the heat release profile at a single transverse location is superimposed. Although the global flames in both configurations have complex structures containing multiple reactions, the three scalars follow similar state relationships in terms of the modified mixture fraction in the two configurations. This

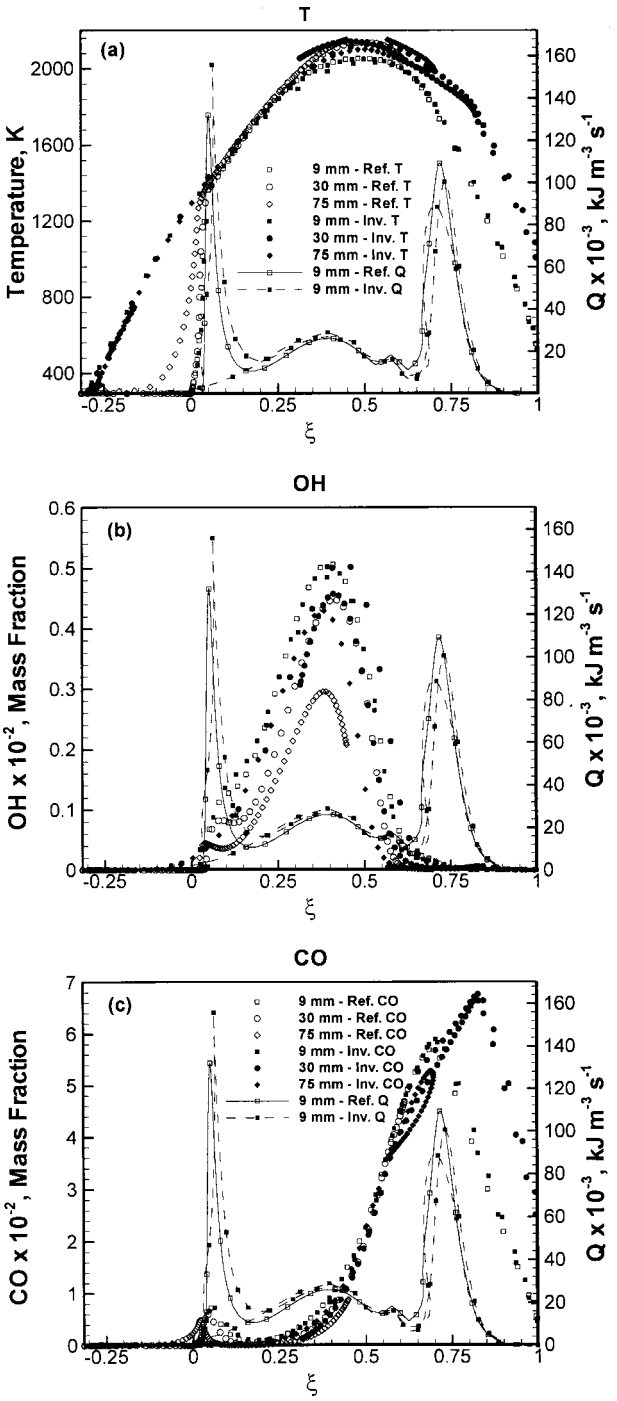

FIG. 10. Similitude between the RC and IC triple flames illustrated by plotting the variation of heat release rate, temperature, and OH and CO mass fractions with respect to the modified mixture fraction at three axial displacements, namely, $Y=9$, 30, and 75 mm. The conditions correspond to those for the flames discussed in the context of Fig. 1.

has important implications for the modeling of partially premixed turbulent combustion, since it appears that it is possible to develop laminar flamelet libraries for partially premixed flames based on the mixture fraction approach. The heat release rate profiles also exhibit good similitude between the two flames, although the magnitude of the heat release peaks differs due to the different overall equivalence ratios in the two configurations.

The scalar profiles clearly illustrate the similitude between the two flames. The three reaction zones in the RC flame are similar to the corresponding five reaction zones of the IC flame in the context of their scalar profiles. The two nonpremixed (or the two rich premixed reaction) zones in the IC flames are not differentiated in terms of ξ. Consequently, the two high temperature peaks are also not discernible.

For both the RC and IC flames, the OH radical profiles indicate that radical activity is highest in the nonpremixed reaction zones where the temperature peaks. Hydroxyl radicals are consumed in the rich premixed zones, but have a non-negligible concentration in the lean premixed zones where oxidizing species are in relative abundance. The CO profiles exhibit two peaks, a larger one on the rich side (in rich premixed zones) and a smaller one in lean premixed reaction zones. This indicates a rapid consumption of CO in lean premixed reaction zones due to the higher oxygen concentrations. The larger peak in the rich premixed reaction zones implies that while CO is produced in the rich-premixed region, it must be transported to the nonpremixed region where it behaves as an intermediate fuel and is oxidized. The CO peak concentration is higher in the RC flame due to the considerably higher value of ϕ_{overall}.

The differences in the state relationships are attributable to the different overall equivalence ratios and the existence of a second nonpremixed reaction zone in the IC flame. For example, the inverse flame contains higher temperatures in both the rich ($0.75<\xi<1.0$) and lean ($\xi\approx 0$) regions. The higher temperature in the rich region is due to the higher overall equivalence ratio for the IC flame, while that in the lean zone is due to a thermal conduction effect involving heat transfer from the second nonpremixed reaction zone (NP2) to the ambient air. Note that the negative values of ξ occur due to the fact that the value of Z_l is based on the nitrogen mass fraction in the lean mixture. Using Z_l corresponding to the ambient conditions will limit ξ between 0 and 1.

F. Transient characteristics of RC and IC flames

Both the RC and IC flames at normal gravity are subjected to a buoyancy-induced global instability that generates large vortex structures, which cause the reaction zones to flicker. We have previously reported the instabilities in the RC flame,[7] in which the flame–vortex interaction involved the outer lean premixed reaction zone. In the IC flame, the buoyancy-induced vortices interact with the outer nonpremixed reaction zone (NP2) to cause large-amplitude oscillations in this zone. This in turn induces large oscillations in the two rich premixed (RP1 and RP2) and the inner nonpremixed (NP1) zones. The absence of coflow adjacent to the outermost slot and a lower Froude number make the IC flame instability stronger and the oscillation amplitude larger than that for the RC flame.

The dynamics of large vortex structures and their interactions with the two flames are investigated by examining a sequence of computed flame images over an oscillation period for both configurations (cf. Fig. 11). In each image, the streaklines are plotted on the left and CHO mass fraction

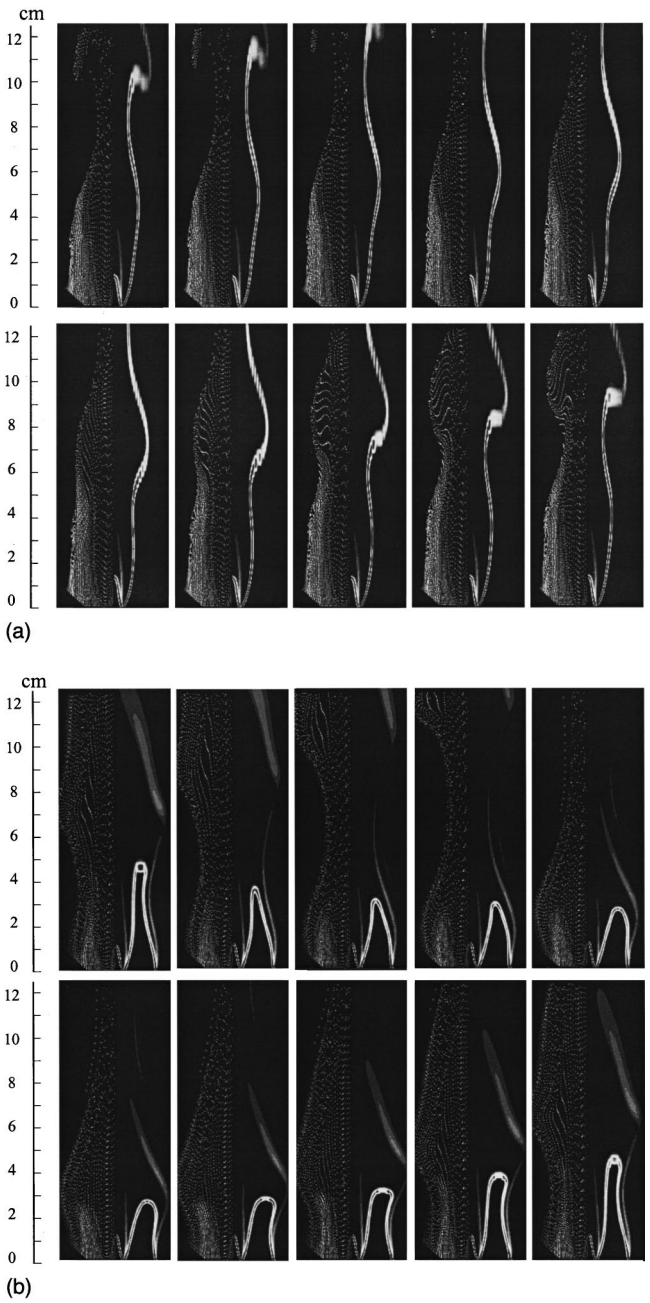

FIG. 11. Instantaneous images of simulated triple flames at five different times within an oscillation period for the RC (top five) and IC triple flames. For each image, the streaklines are plotted on the left-hand side, and CHO contours on the right-hand side.

contours on the right. Due to a significantly reduced concentration of CHO species in the nonpremixed reaction zones, these zones are not as clearly discernible as the rich and lean premixed reaction zones. For the RC flame, the oscillation period is 80 ms and the images are sampled at every 8 ms [cf. Fig. 11(a)]. The three reaction zones appear to be relatively stable at lower axial locations ($Y<52$ mm). At $Y=52$ mm, a large buoyancy-induced vortex is formed. As it moves downstream, it interacts with the lean premixed zone causing large-amplitude oscillations, which in turn induce oscillations in the nonpremixed zone. The inner premixed reaction zone remains relatively unaffected by buoyancy.

The buoyancy-induced instability is relatively stronger in the IC flame due to the smaller value of Fr and the absence of an outer coflow. For the IC flame, the oscillation period is 152 ms and images are sampled every 30.4 ms [cf. Fig. 11(b)]. The inner lean premixed zone (LP) is relatively stable, which is analogous to the behavior of the inner rich premixed zone in the RC flame. On the other hand, the two rich premixed zones (RP1 and RP2) and the outer nonpremixed zone (NP2) exhibit large-amplitude oscillations. The inner nonpremixed zone (NP1) also oscillates in phase with the rich premixed zones but with a smaller amplitude. The vortex rollup occurs at $Y=25$ mm near the outer nonpremixed zone. The flame–vortex interaction is initiated in the nonpremixed reaction zone for the IC flame and in the lean premixed reaction zone for the reference configuration. The flame–vortex interaction is also significantly stronger for the IC flame; as the vortex moves downstream it pinches off the outer nonpremixed reaction surface. Since the highest temperatures occur in the nonpremixed regions, the buoyant acceleration is consequently higher in the IC flame as compared to that in the RC flame.

The computed flame flicker frequencies are 12.5 and 6.6 Hz for the RC and IC and flames, respectively. The lower frequency in case of the IC flame can be attributed to the fact that the Froude number is smaller and the density difference, which is responsible for buoyant acceleration and instability, is larger for this flame. The corresponding measured frequencies for the two cases are 12.5 and 8.5 Hz, respectively. While the predicted and measured frequencies are in agreement for the RC flame, the predicted frequency for the IC flame is $\approx$20% lower compared with the measured value. This discrepancy is most likely due to the absence of coflow in the ambient air. For the reference configuration, the flame is located well inside the outer slot and is relatively shielded from the ambient air due to the coflow in the outer slot. In contrast, the outer nonpremixed reaction zone in the IC flame, which is most influenced by gravity, is located outside the outer slot, and its behavior is strongly influenced by the otherwise quiescent ambient fluid.

G. Effect of equivalence ratios on the flame structure

In Fig. 12 we present the phase-matched experimentally obtained C_2^* chemiluminescent emission images for several cases in order to examine the effects of the rich and lean equivalence ratios on the IC triple flame structure. For all cases the velocities in the inner and outer slots are maintained at 0.3 m s^{-1}. For the top three images, the equivalence ratio in the outer slot is varied, while that in the inner slot is kept constant at $\phi_{\text{lean}}=0.38$. For the bottom three images, ϕ_{lean} is varied while $\phi_{\text{rich}}=1.8$.

As ϕ_{rich} is increased (or the level of partial premixing is reduced in the rich flow), the heights of the two rich premixed reaction zones (RP1 and RP2) increase (due to an increase in the chemical time), their tip opens (at $\phi_{\text{rich}} \approx 1.9$), and the chemical activity (measured by the relative chemiluminescent intensities) in these zones decreases. In contrast, the chemical activity in the two nonpremixed zones (NP1 and NP2) becomes increasingly stronger as ϕ_{rich} is

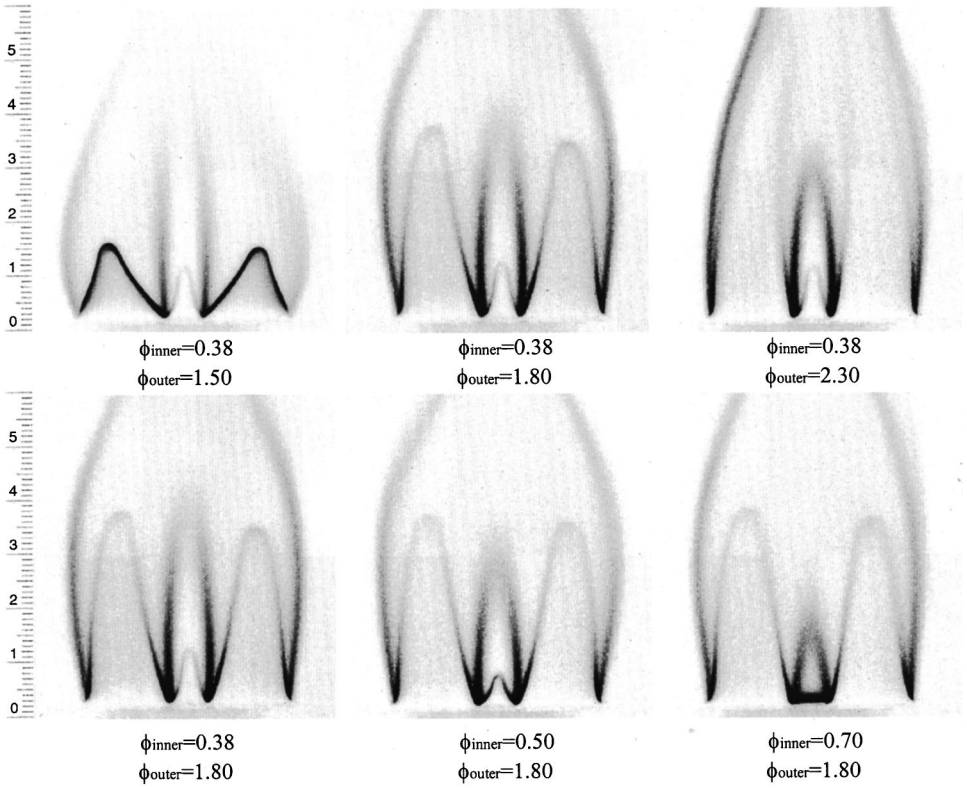

FIG. 12. Phase-matched experimental images of IC triple flames illustrating the effects of variations in rich (outer slot) and lean (inner slot) equivalence ratios, respectively, denoted in the text as ϕ_{rich} and ϕ_{lean}.

increased. At $\phi_{\text{rich}}=2.3$, the two rich premixed reaction zones are almost at the point of merging with their corresponding nonpremixed reaction zones. The lean premixed reaction zone (LP) is relatively unaffected by the variations in ϕ_{rich}. The effect of ϕ_{rich} on the unsteady flame behavior was also investigated. While the oscillation frequency was essentially constant, the oscillation amplitude increased as ϕ_{rich} was increased from 1.5 to 2.3.

The effect of varying ϕ_{lean} on the flame structure is illustrated in the three bottom images of Fig. 12. As expected, the lean premixed reaction zone (LP) is most influenced by variations in the value of ϕ_{lean}. As ϕ_{lean} increases, i.e., as the level of partial premixing in the inner slot is enhanced, the lean premixed zone exhibits greater chemical activity. Since the chemical time decreases as ϕ_{lean} approaches unity, the height of the lean premixed reaction zone (LP) decreases and, consequently, the height of the inner nonpremixed reaction is also reduced. The two rich premixed zones and the outer nonpremixed zone are relatively unaffected by the variation in ϕ_{lean}. The oscillation amplitude and frequency were also found to be essentially insensitive to the variation in ϕ_{lean}.

V. CONCLUSIONS

We have presented the results of a numerical-experimental investigation of methane–air triple flames in two different coflowing configurations. The first configuration (RC) has been considered in many previous investigations, and involves a rich mixture issuing from a central port and a lean mixture from two outer ports. The second configuration (IC) pertains to an inverse of the reference configuration, and contains a lean mixture in the central port and rich mixture in the two outer ports. The IC flames have not been considered in previous studies. For both configurations, flames stabilized on a Wolfhard–Parker slot burner have been investigated in the present study.

While the RC flame contains three reaction zones, the IC flow produces five reaction zones. Our investigation has (1) examined the similitude (and differences) between the RC and IC triple flames in both the spatial and mixture fraction coordinates, (2) compared their unsteady behaviors under normal gravity conditions, and (3) characterized the effects of the rich and lean equivalence ratios on the IC triple flame structure.

Triple flames in the reference and inverse configurations have markedly different spatial structures. The RC flame exhibits a typical triple flame structure with a nonpremixed reaction zone (NP) located in between the rich premixed (RP) and lean premixed reaction zones (LP). In the inverse configuration, the global flame contains five reaction zones. The first three, namely a lean premixed zone (LP), a nonpremixed zone (NP1), and a rich premixed zone (RP1), are stabilized at the thin wall separating the inner and outer slots. These three zones constitute a triple flame that is analogous to the RC triple flame. The outer two reaction zones, i.e., the rich premixed zone (RP2) and the nonpremixed zone (NP2), form a double flame, stabilized at the edge of the outer slot. There is excellent agreement between the predicted and measured topologies of the various reaction zones in both the configurations.

Although the flames in the two configurations have complex global structures containing multiple reactions, their scalar profiles show similar state relationships in terms of the

modified mixture fraction. This has important implications for the modeling of partially premixed turbulent combustion. Minor differences in the state relationships are attributable to the different overall equivalence ratios and the existence of a second nonpremixed reaction zone in the IC flame.

Both the RC and IC flames at normal gravity exhibit well-organized periodic oscillations due to buoyancy-induced instabilities. However, the effect of buoyancy on the IC flame is stronger due to a lower Froude number and absence of coflow for the inverse flame. Moreover, the flame–vortex interactions for the RC flame involves a lean premixed reaction zone, while those for the IC flame involve a nonpremixed reaction zone.

The predicted flame flicker frequencies are 12.5 and 6.6 Hz for the RC and IC flames, respectively. The corresponding measured frequencies for the two cases are 12.5 and 8.5 Hz. While the predicted and measured frequencies are identical for the RC flame, the predicted frequency for the IC flame is $\approx$20% lower compared with the measured value. The discrepancy is attributed to the fact that the RC flame is located well inside the outer slot and is relatively shielded from the ambient air. In contrast, the IC flame is located outside the outer slot, and its behavior is strongly influenced by the otherwise quiescent ambient air.

The effects of the rich and lean equivalence ratios on the IC triple flame structure and its transient characteristics have been investigated. The lean premixed and the inner nonpremixed reactions zones of the IC flame are influenced by variations in ϕ_{lean} in the inner slot. These zones become more reactive as ϕ_{lean} is increased. In contrast, changing ϕ_{rich} affects both the rich premixed and the corresponding nonpremixed reaction zones. The flame oscillation frequency is found to be essentially independent of both ϕ_{rich} and ϕ_{lean}. The oscillation amplitude increases as ϕ_{rich} is increased from 1.5 to 2.3, but is independent of ϕ_{lean}. The differences in the spatial structures and transient characteristics of RC and IC flames lead to different combustion efficiencies for the two flames. The IC flames generally have lower combustion efficiency.

ACKNOWLEDGMENTS

This research was supported by the NASA Microgravity Research Division through Grant No. NCC3-688 for which Dr. Uday Hegde serves as the Technical Monitor. Many fruitful discussions with Dr. V. R. Katta of ISSI are greatly appreciated. We thank Riccardo Azzoni for helping perform the simulations using the SGI workstations at NCSA, Urbana, IL, and Steve Szczap and Chun Choi for assisting with the experiments. Steve Szczap was supported through a NSF Research Experience for Undergraduates grant for which Dr. Farley Fisher is the Program Director.

[1] S. H. Chung and B. J. Lee, ''On the characteristics of laminar lifted flames in a nonpremixed jet,'' Combust. Flame **86**, 62 (1991).
[2] P. N. Kioni, B. Rogg, K. N. C. Bray, and A. Liñán, ''Flame spread in laminar mixing layers. The triple flame,'' Combust. Flame **95**, 276 (1993).
[3] G. R. Ruetsch, L. Vervisch, and A. Liñán, ''Effects of heat release on triple flames,'' Phys. Fluids **7**, 1447 (1995).
[4] Z. Shu, S. K. Aggarwal, V. R. Katta, and I. K. Puri, ''Flame–vortex dynamics in an inverse partially premixed combustor: The Froude number effects,'' Combust. Flame **111**, 276 (1997).
[5] Z. Shu, C. W. Choi, S. K. Aggarwal, V. R. Katta, and I. K. Puri, ''Gravitational effects on the structure of steady two-dimensional partially premixed methane–air flames,'' Combust. Flame **118**, 91 (1999).
[6] R. Azzoni, S. Ratti, S. K. Aggarwal, and I. K. Puri, ''The structure of triple flames stabilized on a slot burner,'' Combust. Flame **119**, 23 (1999).
[7] R. Azzoni, S. Ratti, I. K. Puri, and S. K. Aggarwal, ''Gravity effects on triple flames: Flame structure and flow instability,'' Phys. Fluids **11**, 3449 (1999).
[8] I. S. Wichman and B. Ramadan, ''Theory of attached and lifted diffusion flames,'' Phys. Fluids **10**, 3145 (1998).
[9] T. Echekki and J. H. Chen, ''Structure and propagation of methanol–air triple flames,'' Combust. Flame **114**, 231 (1998).
[10] L. Muniz and M. G. Mungal, ''Instantaneous flame-stabilization velocities in lifted-jet diffusion flames,'' Combust. Flame **111**, 16 (1997).
[11] Y. S. Ko and S. H. Chung, ''Propagation of unsteady tribrachial flames in laminar nonpremixed jets,'' Combust. Flame **118**, 151 (1999).
[12] P. Domingo and L. Vervisch, ''Triple flames and partially-premixed combustion in autoignition of non-premixed turbulent mixtures,'' in *26th International Symposium on Combustion* (The Combustion Institute, Pittsburgh, 1996), pp. 233–240.
[13] P. F. Flynn, R. P. Durrett, G. L. Hunter, A. O. Loye, O. C. Akinyemi, J. E. Dec, and C. K. Westbrook, SAE Paper No. 19990-01-0509, 1999.
[14] J. Chomiak and A. Karlsson, ''Flame liftoff in diesel sprays,'' in Ref. 12, pp. 2557–2564.
[15] Z. Shu, B. J. Krass, C. W. Choi, S. K. Aggarwal, V. R. Katta, and I. K. Puri, ''An experimental and numerical investigation of the structure of steady two-dimensional partially premixed methane–air flames,'' in *27th International Symposium on Combustion* (The Combustion Institute, Pittsburgh, 1998), pp. 625–632.
[16] N. Peters, in *Reduced Kinetic Mechanisms for Applications in Combustion Systems*, Lecture Notes in Physics, Vol. m15, edited by N. Peters and B. Rogg (Springer, Berlin, 1993), pp. 3–14.
[17] R. J. Kee, J. A. Miller, and J. Warnatz, ''A Fortran program package for the evaluation of gas-phase viscosities, conductivities, and diffusion coefficients,'' Sandia National Laboratories Report No. SAND83-8209, 1983.
[18] V. R. Katta, L. P. Goss, and W. M. Roquemore, ''Effect of nonunity Lewis number and finite-rate chemistry on the dynamics of a hydrogen–air jet diffusion flame,'' Combust. Flame **96**, 60 (1994).
[19] R. Azzoni, ''A numerical investigation of methane–air triple flames,'' M.S. thesis, University of Illinois at Chicago, 1999.
[20] S. K. Aggarwal and I. K. Puri, ''Flame structure interactions and state relationships in an unsteady partially premixed flame,'' AIAA J. **36**, 1190 (1998).
[21] F. Takahashi and V. R. Katta, ''Numerical experiments on the vortex–flame interactions in a jet diffusion flame,'' J. Propul. Power **11**, (1995).
[22] H. N. Najm, P. H. Paul, C. J. Mueller, and P. S. Wyckoff, ''On the adequacy of certain experimental observables as measurements of flame burning rate,''Combust. Flame **113**, 312 (1998).